JOURNAL OF PROPULSION AND POWER
Vol. 26, No. 2, March–April 2010

Chemical Nonequilibrium, Heat Transfer, and Friction in a Detonation Tube with Nozzles

Ethan A. Barbour* and Ronald K. Hanson†
Stanford University, Stanford, California 94305

DOI: 10.2514/1.44814

Performance losses in the form of chemical nonequilibrium, heat transfer, and friction are investigated in the context of a detonation tube with nozzles using quasi-one-dimensional computational fluid dynamics. Finite-rate chemistry losses incur up to 10% penalty in overall cycle impulse for mixtures containing fuel and oxygen. These same losses are greatly reduced when oxygen is replaced by air because of reduced energy available through chemical recombination. Heat transfer and friction are less important, both for diverging and converging nozzles (∼5% overall cycle impulse). The exception is for H_2/air where losses can be up to 15%. Finally, a method of predicting losses assuming steady flow nozzles, thereby greatly reducing computational cost, is explored.

I. Introduction

RECENT interest in pulsed detonation engines (PDE) has grown due to the potential advantages in hardware cost and specific impulse over conventional propulsion technologies [1,2]. A PDE operates by burning the reactants via a detonation wave while the pressurized combustion products then generate thrust. This process is repeated in a periodic fashion to achieve quasi-steady thrust. (See Brophy and Hanson [3] for an example of a multicycle PDE.)

However, although PDEs must ultimately operate in a multicycle mode, research has benefited much from single-shot studies. A PDE operated in such a single-shot fashion is often referred to as a detonation tube (DT). Much like the PDE, the DT is filled with a reactant mixture, which is then detonated and produces time-varying thrust. Useful metrics for the DT are its single-shot impulse I and single-shot specific impulse I_{sp}.

Simple, straight DTs have mostly been used to better our understanding of PDEs and their losses. Wintenberger et al. [4] used a semi-analytic/semi-empirical approach to determine scaling laws relevant to DT performance. Cooper and Shepherd [5] extended this work by including the effect of subatmospheric ambient pressures. Cooper et al. [6] and Li and Kailasanath [7] showed that DT specific impulse can be increased by replacing some of the reactants with an inert buffer gas. Losses from simple straight DTs have also been investigated. Radulescu and Hanson [8] used the method of characteristics to show that convective heat transfer losses can be important for certain DT geometries. Owens and Hanson [9] showed that (in addition to heat convection) heat conduction, wall friction and water condensation can all play important roles in DT losses.

The disadvantage to the simple straight DT design is that a significant portion of impulse is lost as pressurized gases expand outside the tube. Therefore, nozzles have been the focus of recent studies to capture some of the lost work potential. Cooper and Shepherd [10] experimentally measured the additional impulse provided by nozzles over a wide range of ambient pressures. Morris [11] and Owens and Hanson [12] used computational approaches to identify optimized area ratios of diverging nozzles for a particular reactant mixture, ambient pressure, and tube geometry. Barbour and Hanson [13] provided a generalized approach for identifying the optimum area ratio of a diverging nozzle for any combination of reactant mixture, ambient pressure, and tube geometry. However, unlike simple straight DTs, the losses from DTs with nozzles have not been investigated. The goal of this work is to fill this gap by focusing specifically on the DT losses which result from the addition of a nozzle.

Three loss mechanisms are addressed. First, chemical nonequilibrium (CNE) is considered. These losses result when the combustion products are not allowed to reach chemical equilibrium (CE) during expansion through a nozzle, thereby inhibiting chemical recombination and its associated heat release. Additional consideration is given to heat transfer losses (which arise from thermal boundary layers which transport thermal energy from the core to the walls), and friction losses (which arise from momentum boundary layers which convert useful kinetic energy into less useful thermal energy). Heat transfer and friction are considered together via Reynolds analogy.

This paper is divided into three major sections. The first section consists of a description of the models used. The second section presents results for losses from diverging nozzles. The third section presents results for losses from a converging nozzle. A short conclusion section then follows.

II. Model Description

A. Computational Model

The unsteady Euler equation is solved in cases which involve no losses. For cases which involve losses, heat transfer, and friction are modeled using simple sink terms, which are discussed more fully in Sec. II.D. The gas is modeled as an ideal gas mixture with variable specific heats. Detailed chemical kinetics are implemented in all cases.

The Euler equation is formulated in 1-D and accounts for variations in the conduit's cross-sectional area. Despite the fact that real detonations are highly 3-D, a 1-D approach is capable of capturing the parameters important to PDEs, such as wave speed, peak pressure, and plateau pressure. Fickett and Davis [[14], see 3A] compared the steady Chapman Jouguet (CJ) theory with experiments and found that the measured speed of the leading shock in a real detonation wave is captured by the 1-D CJ theory to within 2%. Peak wave pressure is not as easily measured as wave speed, so computations are usually performed to address this parameter. As is the case with real 3-D detonations, computations reveal unsteady pressure oscillations behind the leading front, whether the computational model is formulated in one [15] or two [16] dimensions. Furthermore, these studies have shown that the time-averaged pressure behind the leading front is within 1% of the theoretical CJ

Received 8 April 2009; revision received 16 Dec. 2009; accepted for publication 21 Dec. 2009.

*Graduate Research Assistant, High Temperature Gasdynamics Laboratory, Department of Mechanical Engineering, Building 660. Student Member AIAA.

†Clarence J. and Patricia R. Woodard Professor, High Temperature Gasdynamics Laboratory, Department of Mechanical Engineering, Building 520. Fellow AIAA.

pressure. Finally, Owens and Hanson [9] [[17], see 5 and 6] used 2-D computations to show that the well-known analytical Taylor solution for plateau pressure [18] is capable of accurately predicting the time-averaged 2-D solution. The studies described in this paragraph demonstrate that although a 1-D model cannot reproduce the structure of a real detonation wave, it can certainly be used to predict time-averaged pressures, thereby making it a valuable tool for evaluating PDE performance.

In the current model, time integration of the differential equations is performed using a time-step splitting strategy [19]. This approach, which is designed to efficiently handle fluid dynamics and chemistry separately to minimize computational cost, breaks each time step down into a fluid dynamic substep (without chemistry) and a chemistry substep (without fluid dynamics). This time-step splitting approach has been used successfully by others [12,20,21]. The fluid dynamic substep is solved using the weighted essentially non-oscillatory (WENO) method originally proposed by Liu et al. [22].

A full description of the computational scheme can be found in [12,17], and other studies using it can be found in [9,13,21]. The grid is uniform and the chosen grid size is discussed in Sec. III.A. A CFL number of 0.8 was used throughout the current work.

B. Chemical Mechanisms

Three mixtures are considered in this work: $H_2 + 1/2O_2$, $H_2 + 1/2$ air,[‡] and $C_2H_4 + 3O_2$. All H_2/O_2 cases are handled by the H/O submechanism of GRI Mech 3.0 [23] with the $H + O_2 + M$ reaction rate updated for high pressures using Bates et al. [24]. This mechanism contains 8 species and 25 reactions.

The same H/O mechanism is used for the H_2/air cases, where frozen N_2 is also included. Nitrogen chemistry is ignored due to the computational savings associated with a reduced number of species. The H/O system of GRI Mech 3.0 contains 8 species, while the H/O/N system contains 18 species. By freezing nitrogen chemistry, the H_2/air cases are thus modeled using 9 species, which is a significant reduction from 18. To estimate the magnitude of the N_2 chemistry's effect on DT nozzle performance, we consider a steady nozzle with a diverging area ratio of 10, using combustion products of $H_2 + 1/2$ air. The static pressure and temperature at the throat were taken as $P^* = 1.1$ bar and $T^* = 2240$ K, and the exit and ambient pressures were both 0.02 bar. The gas mixture was allowed to reach chemical equilibrium throughout the nozzle. (See Sec. III.E for additional details on calculating chemical equilibrium flow in a steady nozzle). The exit velocity was calculated to be 2271 m/s in the case of full N_2 chemistry, and was 2271 m/s for frozen N_2 chemistry. Since specific impulse is proportional to exit velocity for a steady pressure-matched nozzle, this represents an error of less than 0.1% in I_{sp}.

The reduced mechanism by Varatharajan and Williams [25] was used for all C_2H_4/O_2 cases. Their work specifically targeted ethylene chemistry for use in detonation computations, and is thus directly applicable to the current work. This reduced mechanism has also been used previously on 1-D and 2-D detonation problems by Owens et al. [12,26], Mattison et al. [27], and Tangirala et al. [28]. Because comparisons will be made between CNE and CE, care has been taken to ensure that the proper equilibrium state is recovered with this mechanism. This was done by making all reactions of Varatharajan's mechanism reversible, a strategy also employed in [26,27].

Table 1 summarizes the chemical mechanisms used in the computations.

C. Equilibrium Chemistry

Both CNE and CE are considered in this paper. The CNE solution is obtained by directly implementing the numerical solver as described in [12]. The CE solution, however, requires a slightly different approach.

In light of the time-step splitting scheme used by the model (see Sec. II.A), the method for achieving chemical equilibrium is to simply extend the time allotted to the chemical reaction substep.

[‡]Air represents $O_2 + 3.76N_2$.

Table 1 Summary of chemical mechanisms

Relevant mixture	Number of species	Number of reactions	References	Notes
$H_2 + 1/2O_2$	8	25	[23,24]	GRI Mech 3.0
$H_2 + 1/2$ air	9	25	[23,24]	GRI Mech 3.0 N_2 chemistry frozen
$C_2H_4 + 3O_2$	20	33	[25]	All reactions made fully reversible

If the chemistry is allowed to proceed sufficiently long enough, chemical equilibrium is reached. This approach was tested by computing a flow known to be in CNE using various values for the chemistry substep time t_{chem} and comparing the results to the true CE solution. Since temperature is quite sensitive to the effects of finite-rate chemistry, it was chosen as the metric for evaluating this procedure. Chemical nonequilibrium flow was achieved using a steady conical nozzle with an inlet diameter of 50 mm and a diverging half-angle of 12 deg. The results are compared with the CE flow, which could conceptually be achieved in a sufficiently long diverging nozzle. See Fig. 1.

We first see that the equilibrium solution (black squares) diverges quickly from the finite-rate solution (dotted line). Furthermore, we see that as t_{chem} is increased, the resulting temperature profile approaches the equilibrium solution. For $t_{chem} > 0.1$ s, the equilibrium solution is obtained. A reaction time of $t_{chem} = 10$ s was used in all cases.

There has recently been significant consideration given to the proper evaluation of chemical equilibrium in the context of PDEs and DTs [29,30]. It was pointed out that sound speed (and Mach number) must be evaluated very carefully when the flow is in CE, since the chemical composition adjusts itself within acoustic waves. However, although this is important for analytical solutions (e.g., [13,18], as well as Secs. III.A and III.E of this work) where sound speed plays a major role, the numerical solver used in the current work does not rely on sound speed computations. Rather, the sound speed is adjusted inherently by virtue of the chemical mechanism which shifts the chemical composition according to the local thermodynamic state.

D. Heat Transfer and Friction Models

1. Heat Transfer Model

A simple heat transfer model proposed by Radulescu and Hanson [8] has been used successfully to capture gas velocity [31], species mole fraction [27], and temperature [27] in DTs. However, this model only addresses convective heat transfer and, therefore, underpredicts losses near the end wall where gas velocities are zero and heat conduction is expected to play a major role. Owens and Hanson [9] modified Radulescu's model by incorporating heat

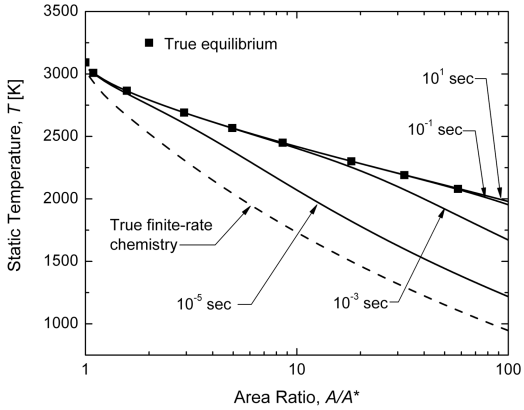

Fig. 1 Determining t_{chem} for achieving CE using steady flow through a conical diverging nozzle. Static temperature is compared for a) true finite-rate chemistry, b) finite-rate chemistry with extended reaction times, and c) true equilibrium. Reactants: $H_2 + 1/2O_2$. Nozzle inlet state: 3093 K, 1.47 bar. For CNE: $D_{inlet} = 50$ mm, $\theta_d = 12$ deg.

conduction as per the analytic solution obtained by Du et al. [32]. This so-called hybrid heat transfer model is used for the current calculations and is described next.

For the most part convective heat transfer is assumed during the DT blowdown and the heat flux is treated as follows:

$$\dot{q}''_{\text{conv}} = -St \cdot \rho \cdot |u - u_w| \cdot (h_{aw} - h_w) \tag{1}$$

where $\dot{q}''_{\text{conv}}$ is the convective heat flux in W/m^2, St is the nondimensional Stanton number, ρ is the static density, u is the gas velocity, u_w is the wall speed (taken as zero in this work), h_{aw} is the static enthalpy which would exist at the wall for adiabatic flow, and h_w is the static enthalpy evaluated at the wall temperature. A commonly used recovery factor for turbulent flow is $Pr^{1/3}$, which leads to the following expression for h_{aw}

$$h_{aw} = h + \frac{1}{2} Pr^{1/3} u^2$$

where h is the static enthalpy in the core. The Prandtl number, Pr, is assumed constant and equal to 0.7.

In the stagnant region which exists between the Taylor expansion wave and the end wall the gas velocity is zero. Here, $\dot{q}''_{\text{conv}}$ is zero and the heat transfer is governed by conduction. The conduction heat flux is expressed as

$$\dot{q}''_{\text{cond}} = -\frac{B_1(\bar{\xi}) \cdot U_{\text{CJ}}^2 \sqrt{\rho_1 \mu_1}}{\sqrt{\bar{\xi}} \sqrt{t}} \tag{2}$$

where $\dot{q}''_{\text{cond}}$ is the heat flux by conduction in W/m^2, U_{CJ} is the detonation wave speed, ρ_1 and μ_1 are the reactant density and dynamic viscosity, respectively, and t is the time after ignition. The nondimensional parameters $\bar{\xi}$ and $B_1(\bar{\xi})$ are functions of the reactant state and are discussed in Owens and Hanson [9]. The values of theses parameters for the mixtures used in this work are listed in Table 2. Heat conduction is assumed to persist until expansion waves from the ambient, or compression waves from a converging nozzle, reach the end wall. Equation (1) is used thereafter at all points in the DT. Heat transfer in nozzles is governed by convection because of the high gas velocities, so Eq. (1) was used for all points in the nozzle at all times.

Both conduction and convection heat transfer models require the wall temperature, T_w, to be specified. The simplest approach is to assume a constant T_w. For a typical DT, the thermal mass of the tube's wall is large enough that T_w stays constant during such a short experiment ($t_{\text{cycle}} \sim 10$ ms). Simulations in this work assume $T_w =$ 500 K. This temperature was chosen since it is representative of typical multicycle PDE wall temperatures. It also eliminates losses associated with water condensation which have been shown to be problematic at room temperature [9].

2. *Friction Model*

When a nonzero bulk flow is present, friction losses are also produced alongside heat transfer losses. Friction results from shear stress at the wall τ_w which itself arises due to a velocity gradient across the tube. These losses are quantified using the nondimensional friction coefficient C_f:

$$\tau_w = \frac{C_f}{2} \cdot \rho \cdot |u - u_w| \cdot (u - u_w) \tag{3}$$

where u_w is again taken as zero in this work. Friction losses directly impact impulse by generating negative shear forces along the side walls of the tube and nozzle. Heat transfer losses, on the other hand, have an indirect effect on impulse since they act to lower the local pressure, which sends expansion waves to the various thrust surfaces, thereby lowering the normal forces on those surfaces.

Table 2 Nondimensional constants used in heat conduction model; $P_1 = 1$ atm; $T_1 = T_w = 500$ K

	$H_2 + 1/2O_2$	$H_2 + 1/2$ air	$C_2H_4 + 3O_2$
$\bar{\xi}$	0.475	0.470	0.486
$B_1(\bar{\xi})$	2.76	1.94	2.20

Owens and Hanson [9] found that the effects of both heat transfer and friction on I_{sp} are of similar magnitude. For example, for their test case of $H_2 + 1/2O_2$ (STP) in a tube with $L/D = 10$, the ideal I_{sp} was calculated to be 193 s. Heat transfer lowered this value by 5 s, while friction lowered it by an additional 4 s.

3. *St and C_f Coefficients*

Equations (1) and (3) are useful only with knowledge of St and C_f. The friction coefficient for flow behind a detonation wave was measured by Edwards et al. [33] who obtained $C_f = 0.0062$. This value has since been used successfully by other researchers [8,26,27] who studied heat transfer and friction losses from DTs, and is therefore adopted here.

The value for St is obtained by appealing to Reynolds analogy, which takes advantage of the symmetry observed by Reynolds between the energy and momentum equations. This relation is shown here in a form which is commonly used for turbulent flows:

$$St = \frac{C_f}{2} \frac{1}{Pr^{2/3}}$$

The friction coefficient and the Stanton number are expected to be, at most, functions of Reynolds number for laminar flow, and nearly constants for turbulent flow. For a $C_2H_4 + 3O_2$ detonation wave (reactants at STP) traveling through a tube of diameter 50 mm, the Reynolds number immediately behind the wave is higher than 10^6. Additionally, the true 3-D nature of the detonation flowfield is expected to further enhance turbulence. Boldman and Graham [34] presented a comprehensive review of heat transfer from nozzles and found that the Stanton number in turbulent flow scales as $St \propto Re^{-1/5}$, a rather weak dependence. Therefore, a constant St and C_f are assumed here.

III. Diverging Nozzles

Gas expansion through diverging nozzles has historically been of interest because of the potential for inducing CNE and thereby suppressing heat release (see Olson [35]). This section explores this problem for DT diverging nozzles. Furthermore, diverging nozzles are expected to have high gas velocities and low densities. Considering the fact that $\dot{q}''_{\text{conv}}$ and τ_w are both proportional to ρu, it is not clear whether losses in a DT's diverging nozzle will be important or not. This section, therefore, also addresses heat transfer and friction.

A. Problem Setup

The DT is shown schematically in Fig. 2. A straight tube of length L_s and diameter D_s is closed at one end. The other end is attached to a conical diverging nozzle with a divergence half-angle of θ_d and length $L_{n,d}$. (Subscript s denotes straight tube, n denotes nozzle, and d denotes diverging.) The straight tube and nozzle are separated by a diaphragm. Initially, quiescent reactants at temperature T_1 and pressure P_1 are to the left of the diaphragm, and quiescent air at T_∞ and P_∞ are to the right. The mixture is ignited at the end wall. This configuration has been used previously by Cooper and Shepherd [10]

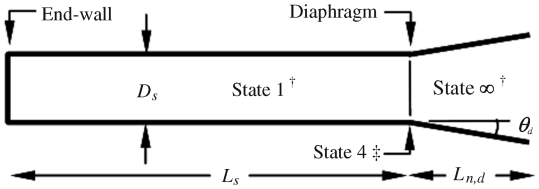

Fig. 2 Schematic of DT with diverging nozzle. † States 1 and ∞ are initial conditions. ‡ State 4 occurs only during steady nozzle flow.

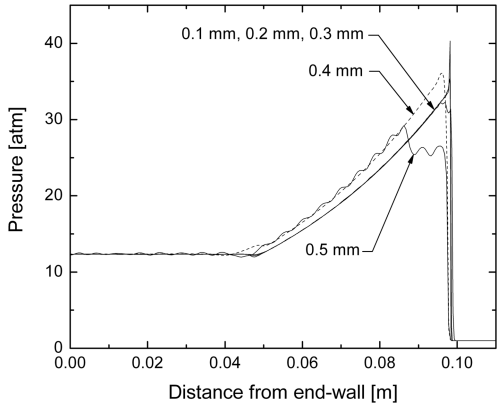

Fig. 3 Grid resolution study. Labels indicate grid cell size. Reactants: $C_2H_4 + 3O_2$, $T_1 = 298$ K, $P_1 = 1$ atm.

to experimentally investigate the performance benefit of DT nozzles over a range of P_∞.

The reactants were ignited by imposing a high temperature/high pressure region in the first 2 mm of the tube. The state of this region was chosen to be 3000 K and 30 atm. (For reference, the CJ state for $C_2H_4 + 3O_2$ is $T_{CJ} = 3950$ K; $P_{CJ} = 19.9$ bar.) It was found that the computed steady detonation wave velocity does not depend on the precise temperature, pressure, or volume this energetic region. A detonation wave forms within 3 mm from this energetic region and travels down the DT at a speed which varies by no more than 1% of its average. Furthermore, this average wave speed was found to be within 1% of the theoretical CJ speed.

The grid resolution was chosen such that a self-sustaining CJ detonation wave could persist from the end wall all the way to the diaphragm. Several grid sizes (0.1, 0.2, 0.3, 0.4, and 0.5 mm) were tested on a DT. The results corresponding to when the leading shock has reached 0.1 m are shown in Fig. 3. With coarse grids, a shock wave propagates but a proper CJ detonation wave is not sustained. This is seen clearly for grid sizes 0.4 mm (where the von Neumann spike is not captured) and 0.5 mm (where the detonation wave has completely failed). On the other hand, grid sizes of 0.3, 0.2, and 0.1 mm are able to sustain a detonation wave out to 0.1 m. At later times when the leading shock is further down the DT, it was found that grid sizes of 0.2 and 0.1 mm are capable of capturing the required detonation to distances beyond 0.5 m, whereas a grid size of 0.3 mm leads to a failed detonation wave shortly after 0.1 m. Since $L_s = 0.5$ m represents the tube length for the majority of calculations covered in this study, a grid size of 0.1 mm was chosen for all cases. After the detonation wave reaches the diaphragm, such a fine grid is no longer needed so the number of grid points was reduced to expedite calculations.

Three reactant mixtures, two divergence angles, and two area ratios were investigated. Table 3 shows the five test cases. A rather large nozzle area ratio ($\varepsilon_d = 100$) was chosen for four of the five cases because this represents the upper limit in terms of practical nozzle area ratios used in rockets. In each case the straight-tube dimensions ($L_s = 0.5$ m; $D_s = 10$ mm) and reactant state ($T_1 = 500$ K; $P_1 = 1$ atm) are unchanged.

The ambient pressure, P_∞, was chosen to match the particular area ratio and reactant mixture of each case. Pressure matching is different for DTs and PDEs than it is for steady jet and rocket engines. For steady engines, the area ratio is chosen such that the nozzle's exit static pressure is equal to the ambient pressure. For unsteady devices such as the DT, an optimized area ratio for a specific ambient pressure is more difficult to identify. Barbour and Hanson [13] found the optimized area ratio, $\tilde{\varepsilon}_d$, as a function of ambient pressure, P_∞. This was done by numerically solving the flowfield at the exit of a DT (without nozzle), and then applying this time-varying solution to analytically predict the nozzle's impulse for any combination of area ratio and ambient pressure. The results were presented using a second order fit, reproduced here:

$$\ell_n(\tilde{\varepsilon}_d) = a_2\left[\ell_n\left(\frac{P_\infty}{P_4^0}\right)\right]^2 + a_1\,\ell_n\left(\frac{P_\infty}{P_4^0}\right) + a_0 \tag{4}$$

where $a_2 = 0.02808$, $a_1 = -0.4618$, and $a_0 = -0.3482$. (This expression was originally presented in a slightly different form in Barbour and Hanson [13], but the relation between $\tilde{\varepsilon}_d$ and P_∞ is faithfully presented using Eq. (4).) The stagnation pressure at state 4, P_4^0, is the stagnation pressure which exists inside the nozzle during the period of steady nozzle flow. It is obtained using

$$P_4^0 = \left(\frac{2}{\gamma+1}\right)^{\frac{\gamma}{\gamma-1}} P_3 \tag{5}$$

where P_3 is the steady pressure at the end wall and is in turn related to the static CJ pressure (see, e.g.,[36], § 1.1.4):

$$P_3 = P_{CJ}\left(\frac{c_3}{c_{CJ}}\right)^{\frac{2\gamma}{\gamma-1}}$$

The sound speed is denoted by c. The steady sound speed at the end wall c_3 is given by:

$$c_3 = \frac{\gamma+1}{2}c_{CJ} - \frac{\gamma-1}{2}U_{CJ}$$

where U_{CJ} is the speed of the CJ detonation wave. The polytropic exponent γ is obtained from the CJ sound speed:

$$\gamma = c_{CJ}^2\frac{\rho_{CJ}}{P_{CJ}} \tag{6}$$

Notice that because the CJ state is typically at such elevated temperatures and pressures, the CJ sound speed, c_{CJ}, is the chemically equilibrated sound speed. This implies that γ is not equal to the ratio of specific heats. All CJ properties (c_{CJ}, U_{CJ}, P_{CJ}, γ) were obtained using STANJAN [37]. Values for γ are listed in Table 3. Note that γ is only useful here for evaluating P_∞. The numerical model used for solving the unsteady flowfield does not make use of γ.

B. Performance Metrics

The time-varying thrust of a DT is determined by all forces (both pressure and shear) acting throughout the control volume. These forces have been broken down into four components: the pressure force in the straight tube (F_s^{press}), the pressure force in the nozzle (F_n^{press}), the shear force in the straight tube (F_s^{shear}), and the shear force in the nozzle (F_n^{shear}). These forces are depicted in Fig. 4. Notice that the DT is broken down into two distinct sections: straight tube and nozzle.

The forces are added together to determine the net straight-tube thrust $\mathcal{T}_s$ and the net nozzle thrust $\mathcal{T}_n$:

Table 3 Test cases for DT with diverging nozzle; in all cases, $L_s = 0.5$ m, $D_s = 10$ mm, $T_1 = T_w = 500$ K, and $P_1 = 1$ atm

Case	Mixture	Area ratio, ε_d	Divergence angle, θ_d, deg	γ	P_3, bar	P_4^0, bar	P_∞, Pa
1	$H_2 + 1/2O_2$	100	12	1.13	4.38	2.54	155
2	$H_2 + 1/2$ air	100	12	1.16	3.77	2.16	132
3	$C_2H_4 + 3O_2$	100	12	1.14	7.39	4.26	265
4	$H_2 + 1/2O_2$	100	5	1.13	4.38	2.54	155
5	$H_2 + 1/2O_2$	10	12	1.13	4.38	2.54	2800

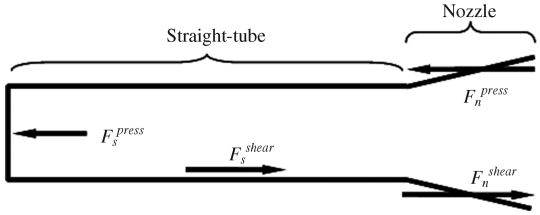

Fig. 4 Breakdown of forces in DT with diverging nozzle.

$$\mathcal{T}_s(t) \equiv F_s^{\text{press}}(t) + F_s^{\text{shear}}(t) \tag{7}$$

$$\mathcal{T}_n(t) \equiv F_n^{\text{press}}(t) + F_n^{\text{shear}}(t) \tag{8}$$

Once the net thrusts are determined they are integrated to obtain the straight-tube impulse I_s and the nozzle impulse I_n:

$$I_s \equiv \int \mathcal{T}_s(t)\,\mathrm{d}t \tag{9}$$

$$I_n \equiv \int \mathcal{T}_n(t)\,\mathrm{d}t \tag{10}$$

where integration ends when the end-wall pressure has reached P_∞. Overall impulse is the sum of two preceding impulses:

$$I \equiv I_s + I_n \tag{11}$$

Finally, we are interested in comparing the impulse in the presence of losses, I, with the ideal impulse, I_{ideal}. The impulse efficiency is defined as

$$\eta_{\text{impulse}} \equiv \frac{I}{I_{\text{ideal}}}$$

and is the metric used to evaluate the various DT losses. In all cases I_{ideal} is achieved by setting $\dot{q}'' = 0$ (no heat transfer), $\tau_w = 0$ (no friction), and $t_{\text{chem}} = 10$ s (chemical equilibrium; see Sec. II.C).

C. Losses Because of Chemical Nonequilibrium

1. Time-Varying Forces

Losses due to CNE are investigated in this section. Heat and friction are ignored ($\dot{q}'' = \tau_w = 0$). It was found that departures from equilibrium chemistry in the straight tube were negligible, and, therefore, the effects of finite-rate chemistry on the straight-tube force F_s^{press} were also small. This is consistent with the findings of Mattison et al. [27], who showed that the gases in a simple straight DT are in chemical equilibrium ($C_2H_4 + 3O_2$, $P_1 = 1$ atm). Therefore, the simulations in this work were performed with CE in the straight tube. Both CE and CNE were considered in the nozzle.

Figure 5 shows the force histories for case 1. Panel (a) contains the straight-tube force, F_s^{press}, and panel (b) contains the nozzle force, F_n^{press}.

Panel (a) shows the time-varying force from the straight tube. At approximately 0.2 ms the diaphragm breaks. This is accompanied by a sudden rise in force. The reason for this rise is that while the detonation wave is traversing the straight-tube there is a negative thrust surface provided by the diaphragm, so the force increases from $A_s(P_3 - P_1)$ to $A_s(P_3 - P_\infty)$ after the diaphragm breaks. (A_s is the cross-sectional area of the straight tube.) Panel (a) shows that altering the chemistry in the nozzle does not affect the straight-tube force history (the solid and dashed lines are indistinguishable from each other). This is expected based on the finding of Owens and Hanson [12] who showed that even a purely diverging nozzle in a DT is choked, meaning that the straight-tube flowfield is unaffected by what happens in the nozzle.

Panel (b) shows the time-varying forces from the nozzle. As the Taylor wave passes through the nozzle, the nozzle force rises to nearly 70 N and then falls. It reaches a steady state which persists between 0.3 and 0.8 ms, after which the nozzle blows down. (See

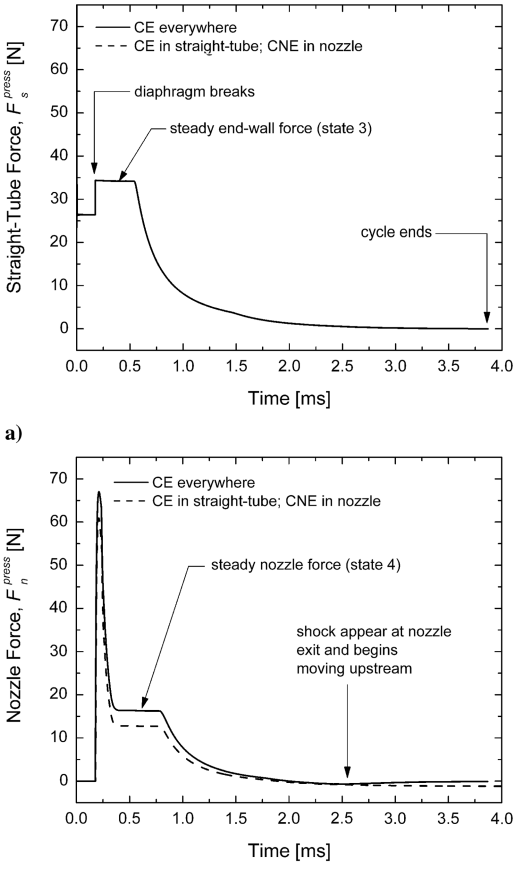

Fig. 5 Force histories for case 1 showing losses due to CNE. Panel (a): straight-tube force. Panel (b): nozzle force. CNE is allowed only in the nozzle. Shear forces and heat transfer are zero.

Barbour and Hanson [13] for more details on the nozzle thrust behavior.) The figure clearly shows an effect from finite-rate chemistry on the nozzle force, which in turn reduces the nozzle impulse, I_n. The reason for this can be understood in terms of heat release. At typical CJ conditions there exists large amounts of O, H, H_2, OH and (for hydrocarbons) CO. All of these species can recombine when they cool to the more familiar combustion products H_2O and CO_2. This recombination releases heat, raising the temperature and pressure, and consequently thrust and specific impulse. If expansion takes place quickly enough so that these species remain frozen this additional heat is not released and performance suffers. Further details on the theory can be found in Vincenti and Kruger [38] (section 8) or Penner [39] (section 3).

Table 4 summarizes impulse results for all cases.

2. Discussion

A few key conclusions can be gleaned from Table 4. First, we notice that for the same nozzle geometry the H_2/O_2 mixture (case 1) and C_2H_4/O_2 mixture (case 3) suffer similar losses (9%), whereas the H_2/air mixture (case 2) suffers a much smaller loss (2%). Note that H_2/air combustion takes place at much lower temperatures than H_2/O_2 and C_2H_4/O_2 combustion, which would lead to the expectation that the H_2/air mixture should be more susceptible to CNE than the H_2/O_2 and C_2H_4/O_2 mixtures. Although this is true, the reason for the small losses with H_2/air is that the heat released by chemical recombination in the nozzle must go into raising the pressure and temperature of all products, including nitrogen. In other words, dilution from inert nitrogen reduces the relative effect of chemical recombination. For mixtures which do not contain nitrogen, there are more radicals with the potential for heat release in the nozzle. While studying CNE effects in scramjets, Sangiovanni et al. [[40], Table 3 ($C_s = 0.988$)] also observed only very small

Table 4 Results of CNE loss (see Table 3 for a description of each case); heat transfer and friction are zero throughout

	No losses			Losses in nozzle			
	Straight tube, I_s, N · ms	Nozzle, I_n, N · ms	Total, I, N · ms	Straight tube, I_s, N · ms	Nozzle, I_n, N · ms	Total, I, N · ms	Impulse efficiency, η_{impulse}
Case	(a)	(b)	(c) = (a) + (b)	(d)	(e)	(f) = (d) + (e)	(f)/(c)
1	29.4	18.2[a]	47.6	29.4	14.2[a]	43.5	0.91
2	34.5	14.3	48.8	34.5	13.5	48.0	0.98
3	62.3	38.8	101	62.3	30.0	92.3	0.91
4	29.7	18.5	48.2	29.7	14.7	44.4	0.92
5	29.0	9.65	38.7	29.0	8.06	37.1	0.96

[a]For case 1, a shock entered the nozzle when losses were absent but did not when losses were present. For the sake of comparison, therefore, impulse integration was terminated early at $t = 2.5$ ms, both with and without losses.

thrust losses (∼1%) associated with chemical recombination of the H_2/air products.

Next we consider the effect of elongating the nozzle by comparing a divergence half-angle of 12 deg (case 1) with a half-angle of 5 deg (case 4). The reason for elongating the nozzle is to provide a longer residence time to the gases, thus giving more opportunity for chemical recombination to take place. Indeed, we find that the performance improves for the 5 deg nozzle, but this improvement is only marginal (8% for 5 deg vs 9% for 12 deg). The implication is that it may be impossible to avoid losses by finite-rate chemistry for nozzles of practical divergence angles and lengths.

Finally, we consider the effect of reducing the area ratio, which would be required in practice for either higher ambient pressures or lower reactant pressures. Case 1 has an area ratio of 100 and an ambient pressure of 155 Pa, while case 5 has an area ratio of 10 and an ambient pressure of 2800 Pa. By considering a higher ambient pressure (and thereby a smaller area ratio) the losses are reduced from 9% to 4%. This is because the pressures and temperatures encountered in the $\varepsilon_d = 10$ nozzle are not as low as those encountered in the $\varepsilon_d = 100$ nozzle, and so departures from chemical equilibrium are not as great for $\varepsilon_d = 10$.

D. Losses Because of Heat Transfer and Friction

1. *Time-Varying Forces*

The same cases defined in Table 3 were simulated again, this time allowing losses by heat transfer and friction. Chemical equilibrium was imposed in all cases. Recall that the preceding section only considered losses in the nozzle. In the case of heat transfer and friction, however, it is known that these losses can play an important role in reducing the impulse of a simple straight DT [8,9]. Thus, calculations in this section were performed for (i) ideal flow in straight tube/ideal flow in nozzle, (ii) ideal flow in tube/losses in nozzle, and (iii) losses in tube/losses in nozzle. The results were used to determine the relative role of losses from the straight tube, versus losses from the nozzle.

Figure 6 shows the force histories for case 1. Panel (a) contains the straight-tube pressure force (F_s^{press}) and shear force (F_s^{shear}). Panel (b) contains the nozzle pressure force (F_n^{press}) and shear force (F_n^{shear}). The force histories corresponding to ideal flow are identical to the ideal flow results in Fig. 5.

Panel (a) shows the time-varying straight-tube forces. As with CNE-induced losses of Sec. III.C, heat transfer and friction losses which occur in the nozzle do not affect the straight-tube flowfield. When losses in the straight tube are allowed, the pressure force decays and the shear force becomes nonzero. We see that losses in the straight tube lead to a large drop in straight-tube impulse, I_s.

Panel (b) shows the time-varying nozzle forces. Note that when only nozzle losses are allowed, the change in pressure force (F_n^{press}) is so slight that the effect cannot be resolved in the figure. This is because the static pressure is largely unaffected by losses. This may seem unexpected, but can be explained by appealing to Rayleigh and Fanno flow theories (see, e.g., [41]). Rayleigh theory (which deals with heat transfer in the absence of friction) predicts that the Mach number moves away from unity for heat loss, while Fanno theory (which deals with friction in the absence of heat transfer) predicts that the Mach number moves toward unity. These Mach number trends result in a static pressure drop from Rayleigh flow (heat transfer) and a static pressure rise from Fanno flow (friction). The net result can therefore be either a drop or a rise in F_n^{press}. In fact, the data actually exhibit a very slight increase in F_n^{press} (not discernible in the figure). However, this does not imply improved nozzle performance (which would be a violation of the second law of thermodynamic) since now the shear force F_n^{shear} is nonzero. The net effect is a drop in nozzle thrust $\mathcal{T}_n$. Finally, we see that when losses from the straight tube are also included, these exacerbate losses in the nozzle by severely reducing the pressure force (gray line).

Table 5 summarizes impulse results for all cases. Note that each value for impulse (I_s, I_n, and I) contains both pressure and shear contributions, as per Eqs. (7–11).

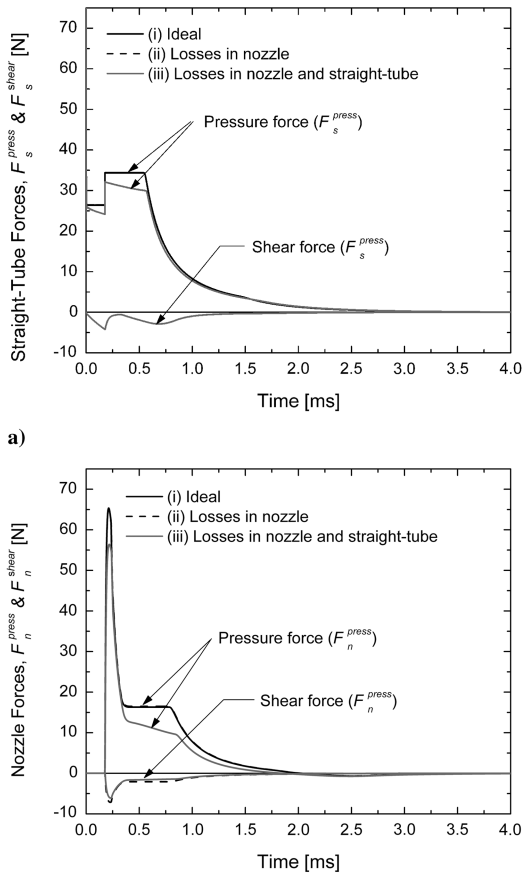

Fig. 6 Force histories for case 1 showing losses due to heat transfer and friction. Panel (a): straight-tube forces. Panel (b): nozzle forces. Chemical equilibrium is used in all calculations.

2. Discussion

The preceding table has two columns listing the impulse efficiency η_{impulse}. We start by focusing on the simulations which include only losses in the nozzle, i.e., η_{impulse} in section (ii) of Table 5. The losses for the three mixtures (cases 1–3) are all quite similar (4–5%), unlike the results of the CNE calculations which showed very different losses depending on whether or not nitrogen was included. When the divergence angle is reduced (case 4), the losses are enhanced (11% for 5 deg vs 5% for 12 deg). This is because a smaller divergence angle corresponds to a longer nozzle, and such a nozzle has more surface area for friction and heat transfer to act upon. Recall from Sec. III.C that lengthening the nozzle has the effect of reducing CNE-induced losses, so this represents a tradeoff between CNE losses and heat/friction losses. However, the improvement in CNE-induced losses observed by lengthening the nozzle was marginal. Thus, a shorter nozzle should be preferred from the point of view of minimizing heat transfer and friction losses. Finally, a nozzle with a smaller area ratio (case 5) has smaller losses (3%) than a nozzle with a larger area ratio (5%, case 1). As was the case for the divergence angle, this improved performance is due to a reduced surface area.

Next we turn our attention to simulations which include losses both in the nozzle and the straight tube, i.e., η_{impulse} in section (iii) of Table 5. In general we find that these losses tend to be much larger than the losses which occur from the nozzle alone. This implies that diverging nozzles play only a small role in overall DT losses from heat transfer and friction. It is also worth noting that the largest losses come from the H_2/air mixture (case 2). The reason for this is two fold. First, the end-wall pressure P_3 is lower for H_2/air than for the other mixtures (see Table 3), which leads to a more pronounced loss as this force decays. Second, the sound speed throughout the products of H_2/air is quite low (due to the low combustion temperatures), and this results in a prolonged blowdown which in turn allows more heat to be lost. These large losses for H_2/air will be encountered again when exploring converging nozzles.

E. Predicting Losses Using a Steady Nozzle

This section describes how an estimate of losses from a DT's diverging nozzle can be made using a steady nozzle assumption. We do so by appealing to the steady nozzle flow which exists in a DT (see Fig. 5b between 0.3 and 0.8 ms). This steady flow was derived by the authors in a previous work [13] and was labeled state 4. We now use state 4 as the choked inlet of a steady diverging nozzle and evaluate losses for the five cases listed in Table 3. The stagnation pressure at state 4 is listed in Table 3 for each mixture. The static pressure at state 4 can be derived using Eq. (5):

$$P_4 = \left(\frac{2}{\gamma+1}\right)^{\frac{2\gamma}{\gamma-1}} P_3$$

The remaining variables are obtained by isentropically expanding from the CJ pressure to P_4 using an equilibrium calculator (e.g., STANJAN [37]). For example, state 4 for $H_2 + 1/2O_2$ ($P_1 = 1$ atm; $T_1 = 500$ K) consists of the following: $P_4 = 1.47$ bar, $T_4 = 3093$ K, $\rho_4 = 0.0866$ kg/m^3, $u_4 = c_4 = 1375$ m/s, and $h_4 = -0.648$ MJ/kg. The stagnation enthalpy is $h^0 = h_4 + 1/2u_4^2 = 0.297$ MJ/kg. For an inlet diameter of 10 mm, the mass flow rate is $\dot{m} = 0.00935$ kg/s.

Having established the relevant inlet state to the nozzle, it is now necessary to find the exit state. For a nozzle without losses this is done quite easily by iteratively expanding the gas from P_4, evaluating the area ratio, and repeating until the desired area ratio is reached. For the H_2/O_2 mixture considered in the preceding paragraph, we expand to $P_{\text{exit}} = 263$ Pa. Using STANJAN this corresponds to $\rho_{\text{exit}} = 2.81 \cdot 10^{-4}$ kg/m^3 and $h_{\text{exit}} = -8.71$ MJ/kg. By keeping the stagnation enthalpy constant, we find $u_{\text{exit}} = 4244$ m/s. Using ρ_4, u_4, ρ_{exit}, and u_{exit} the area ratio is computed as $\varepsilon_d = 100$, the desired value for case 1. If the flow is not ideal (i.e., if CNE, heat transfer or friction are present), then the equations of mass, momentum, energy, and species must be integrated from state 4 to obtain the nozzle exit state. See Cooper [42] (chapter 6) for solving nozzle flow with finite-rate

Table 5 Results of heat transfer and friction (see Table 3 for a description of each case); chemical equilibrium is enforced throughout

	(i) No losses			(ii) Losses in nozzle				(iii) Losses in nozzle and straight tube			
	Straight tube, I_s, N · ms	Nozzle, I_n, N · ms	Total, I, N · ms	Straight tube, I_s, N · ms	Nozzle, I_n, N · ms	Total, I, N · ms	Impulse efficiency, η_{impulse}	Straight tube, I_s, N · ms	Nozzle, I_n, N · ms	Total, I, N · ms	Impulse efficiency, η_{impulse}
Case	(a)	(b)	(c) = (a) + (b)	(d)	(e)	(f) = (d) + (e)	(f)/(c)	(g)	(h)	(j) = (g) + (h)	(j)/(c)
1	29.7	18.1	47.8	29.7	15.8	45.5	0.95	25.3	11.4	36.7	0.77
2	34.8	14.1	48.9	34.9	11.7	46.6	0.95	25.8	6.11	31.9	0.65
3	62.9	38.5	101	62.9	33.6	96.5	0.96	54.6	27.3	81.9	0.81
4	29.7	18.5	48.2	29.7	13.3	43.0	0.89	25.3	9.26	34.6	0.72
5	29.0	9.65	38.7	29.0	8.69	37.7	0.97	24.5	6.20	30.7	0.79

chemistry, and Oosthuizen and Carscallen [41] (chapter 11) for solving nozzle flow with heat transfer and friction. For the case of finite-rate chemistry, we obtain $P_{\text{exit}} = 145$ Pa and $u_{\text{exit}} = 3972$ m/s.

With the exit state in hand, the thrust of the steady nozzle is obtained using the following equation:

$$\mathcal{T}_{\text{steadynozzle}} = \dot{m} \cdot u_{\text{exit}} + A_{\text{exit}}(P_{\text{exit}} - P_{\infty})$$

Recall that the nozzle is not pressure matched, since this would disturb the optimized DT performance. Taking the ambient pressure obtained from Eq. (4) (i.e., $P_{\infty} = 155$ Pa), the ideal steady nozzle thrust works out to 40.5 N for the H_2/O_2 example being considered here. In the case of CNE, the computed thrust is 37.1 N.

An important observation is now made: by taking the ratio of nonideal thrust to ideal thrust for the steady nozzle (i.e., $37.1 \div 40.5 = 0.92$), we nearly recover the ratio of nonideal impulse to ideal impulse for the DT, i.e., 0.91 (Table 4, case 1). The latter has already been termed the impulse efficiency, η_{impulse}, and the former is now termed the thrust efficiency, η_{thrust}. Because state 4 persists for a sufficient amount of time during the DT blowdown, losses in impulse from the unsteady DT can be approximated using a steady nozzle with an inlet state equal to state 4. In other words, $\eta_{\text{impulse}} \approx \eta_{\text{thrust}}$.

Figure 7 compares η_{impulse} with η_{thrust} for all five cases. Finite-rate chemistry losses are shown using open symbols, and heat/friction losses are shown using closed symbols. The values for η_{impulse} are taken from Tables 4 and 5 [section (ii)]. The values for η_{thrust} are calculated from steady nozzle flow. Losses from the straight tube are neglected throughout. We see that there is excellent agreement between the two efficiencies.

The huge computational savings of using this steady nozzle approach allows easy estimation of DT nozzle losses over a wide range of conditions. For example, rather than restricting ourselves to a few combinations of θ_d and ε_d, steady nozzle calculations can be easily performed to estimate losses over a wide range of geometrical configurations. One could also depart from the conical nozzle shape adopted here in favor of, for example, a deLaval nozzle. Different fuels and equivalence ratios can also be easily explored. In addition, reduced chemical mechanisms can be abandoned in favor of complete mechanisms.

IV. Converging Nozzles

The preceding section dealt exclusively with purely diverging nozzles. These types of nozzles were able to incur two types of losses: 1) CNE losses due to the freezing of combustion products, and 2) heat/friction losses which act along the nozzle walls. This section will focus on a converging nozzle. Converging nozzles are important for maintaining a particular state in the PDE combustor during refresh. Because pressures and temperatures are still quite high in a converging nozzle, CNE losses are not expected to be important and are therefore ignored here. Therefore, heat transfer and friction will be the focus of this section.

The same mixtures which were explored in the context of diverging nozzles will again be investigated here. However, a different approach will be taken for the DT geometry. The mechanism for heat/friction loss from a DT with a converging nozzle is different from a DT with a diverging nozzle. The diverging nozzle provides extra surfaces at which losses can occur. Converging nozzles, however, tend to be quite short and, therefore, are not expected to directly contribute much to losses. Rather, the converging nozzle acts to increase the residence time of hot moving gases inside the straight tube by restricting the outflow. This effect in turn enhances the losses from the straight tube. For example, Cooper and Shepherd [10] measured impulse using a ballistic pendulum and observed a 27% drop in impulse when a converging section was added. They attributed some of this to enhanced heat/friction losses resulting from the prolonged blowdown. Thus, in this section the nozzle geometry will be fixed and the straight-tube geometry will be varied.

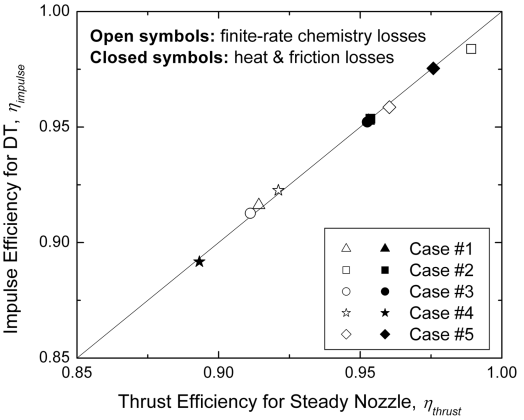

Fig. 7 Comparing η_{impulse} with η_{thrust}. Open symbols: CNE losses. Closed symbols: heat/friction losses. Losses in straight tube were neglected.

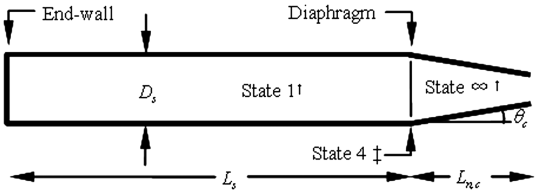

Fig. 8 Schematic of DT with converging nozzle. † States 1 and ∞ are initial conditions.

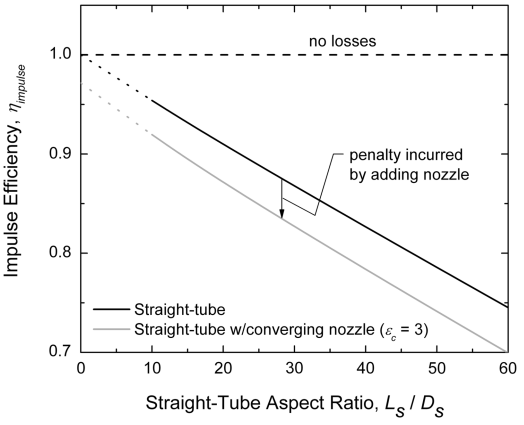

a)

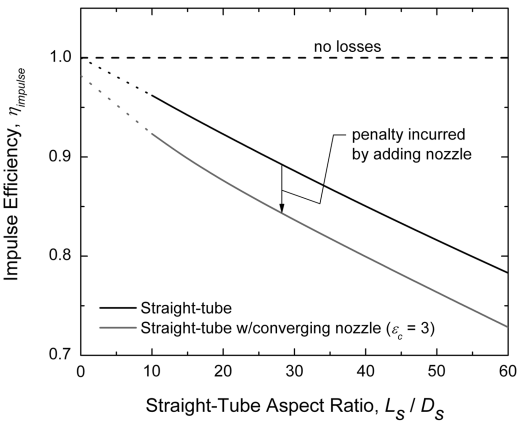

b)

Fig. 9 Impulse efficiency as a function of L_s/D_s and L_s. Panel (a) $L_s = 0.5$ m, Panel (b) $L_s = 1$ m. $H_2 + 0.5O_2$.

Table 6 Impulse efficiency for DT without nozzle; $L_s = 0.5$ m and $D_s = 10$ mm

	No losses	With losses	
	Straight tube, I_s, N · ms	Straight tube, I_s , N · ms	Impulse efficiency, η_{impulse}
Mixture	(a)	(b)	(b)/(a)
$H_2 + 1/2O_2$	18.6	14.6	0.78
$H_2 + 1/2$ air	20.9	14.5	0.69
$C_2H_4 + 3O_2$	46.4	38.1	0.82

A. Problem Setup

The conditions in this section are mostly the same as for the diverging nozzle calculations. The initial state is $P_1 = 1$ atm and $T_1 = 500$ K, and the wall temperature is 500 K. The ambient pressure is $P_\infty = 1$ atm. The DT setup is shown in Fig. 8. The subscript c is used to denote converging, as in $L_{n,c}$, ε_c, and θ_c. Again, reactants are initially to the left of the diaphragm, and air is to the right. The reactants are ignited at the end wall. As with the diverging nozzle, the grid resolution was 0.1 mm before the detonation wave reached the diaphragm and made coarser thereafter. Because of the high T and P, chemical equilibrium is imposed throughout.

The nozzle has a converging area ratio, ε_c, of 3. This area ratio is equal to that of well-known rocket engines, such as the RL-10 and the SSME (see [43], Table 11.4). The ratio of the nozzle length to straight-tube diameter, $L_{n,c}/D_s$, has a value of two for all configurations so that there are enough grid points in the nozzle.

B. Varying Geometry

We begin by varying L_s/D_s (which is known to be an important determinant of losses [8]) and L_s. Figure 9 shows the impulse efficiency over a range of L_s/D_s both without and with the nozzle. The length of the straight tube L_s is 0.5 m in panel (a) and 1 m in panel (b). Calculation results are represented by solid lines. These are extrapolated down to $L_s/D_s = 0$ with dotted lines.

For the straight tube (black lines) we see that the losses increase linearly as L_s/D_s increases, as was also observed by Radulescu and Hanson [8]. By adding the nozzle (gray lines), more losses are experienced at all values of L_s/D_s, and the line shifts down. This added loss is approximately 5% in all cases, which means that for $L_s/D_s \sim 10$ the losses are doubled when the nozzle is added.

Notice that the impulse efficiency is much more sensitive to L_s/D_s than it is to L_s. This is true for both the straight tube and the straight tube with converging nozzle configurations. In the case of the straight tube without nozzle, the flowfield is self similar in L_s/D_s [8]. By adding the nozzle the flowfield is no longer self similar, but we see that L_s/D_s remains the most influential factor in terms of determining heat/friction losses.

C. Varying Mixture

The following two tables show results for each of the three reactant mixtures. Table 6 shows the effect of losses on a DT without nozzle. Table 7 shows the effect of losses on a DT with converging nozzle. By comparing the two tables we can see the effect that adding the nozzle has on losses.

The losses with a mixture of H_2/O_2 and C_2H_4/O_2 are quite similar to each other, and adding a nozzle has a similar effect on both mixtures (∼5% additional losses). On the other hand, the mixture of H_2/air leads to noticeably more losses, and the addition of a nozzle incurs the greatest drop in impulse (14% additional losses). The reasons for these enhanced losses for H_2/air are the same as in Sec. III.D which addressed diverging nozzles: H_2/air has a lower P_3, which exacerbates the pressure decay at the end wall; furthermore this mixture has a reduced sound speed, which prolongs the cycle and provides more time for energy to be lost.

V. Conclusions

This paper described simulations which were designed to investigate the effects that nozzles have on DT losses. First, diverging nozzles were considered, and losses arising due to CNE, heat transfer and friction were quantified. Next, converging nozzles were considered, and heat transfer and friction losses were quantified (CNE losses being assumed negligible).

Losses from CNE occur because of the suppressed chemical recombination. Losses from heat transfer and friction take place at the walls; the diverging nozzle itself leads directly to losses, whereas the converging nozzle traps gases inside the straight tube which itself experiences greater losses as a result.

In the case of CNE losses the important findings included 1) losses are ∼10% for O_2 mixtures, 2) losses are unimportant for air mixtures, 3) lengthening nozzle improves performance only slightly, and 4) losses are greatest for large ε_d. In the case of heat transfer and friction losses, the important findings included 1) losses are ∼5% for O_2 mixtures, 2) losses are ∼15% for air mixtures, 3) losses are sensitive to length of diverging nozzle, and 4) losses are greatest for large ε_d.

Thus, CNE losses are expected to be the dominant loss mechanism for rocket PDEs, whereas heat transfer and friction the dominant loss mechanism for air-breathing PDEs.

Additionally, it was shown that steady nozzle calculations can reliably predict the magnitude of losses experienced by a DT's diverging nozzle if state 4 is used for the steady nozzle's inlet.

Acknowledgment

This work was supported by the Office of Naval Research, with Gabriel Roy serving as technical monitor.

References

[1] Roy, G. D., Frolov, S. M., Borisov, A. A., and Netzer, D. W., "Pulse Detonation Propulsion: Challenges, Current Status, and Future Perspective," *Progress in Energy and Combustion Science*, Vol. 30, No. 6, 2004, pp. 545–672. doi:10.1016/j.pecs.2004.05.001

[2] Kailasanath, K., "Research on Pulse Detonation Combustion Systems —A Status Report," *47th AIAA Aerospace Sciences Meeting*, AIAA Paper 2009-631, 2009.

[3] Brophy, C. M., and Hanson, R. K., "Fuel Distribution Effects on Pulse Detonation Engine Operation and Performance," *Journal of Propulsion and Power*, Vol. 22, No. 6, 2006, pp. 1155–1161. doi:10.2514/1.18713

Table 7 Impulse efficiency for DT with converging nozzle; $L_s = 0.5$ m, $D_s = 10$ mm, and $\varepsilon_c = 3$

	No losses			With losses			
	Straight tube, I_s, N · ms	Nozzle, I_n, N · ms	Total, I, N · ms	Straight tube, I_s, N · ms	Nozzle, I_n, N · ms	Total, I, N · ms	Impulse efficiency, η_{impulse}
Mixture	(a)	(b)	(c) = (a) + (b)	(d)	(e)	(f) = (d) + (e)	(f)/(c)
$H_2 + 1/2O_2$	39.1	−21.5	17.6	28.2	−15.2	13.0	0.74
$H_2 + 1/2$ air	42.2	−23.0	19.2	22.4	−11.7	10.7	0.56
$C_2H_4 + 3O_2$	101	−57.2	44.2	78.4	−44.2	34.2	0.77

[4] Wintenberger, E., Austin, J. M., Cooper, M., Jackson, S., and Shepherd, J. E., "Analytical Model for the Impulse of Single-Cycle Pulse Detonation Tube," *Journal of Propulsion and Power*, Vol. 19, No. 1, 2003, pp. 22–38. doi:10.2514/2.6099

[5] Cooper, M., and Shepherd, J. E., "Detonation Tube Impulse in Subatmospheric Environments," *Journal of Propulsion and Power*, Vol. 22, No. 4, 2006, pp. 845–851. doi:10.2514/1.16979

[6] Cooper, M., Shepherd, J. E., and Schauer, F., "Impulse Correlation for Partially Filled Detonation Tubes," *Journal of Propulsion and Power*, Vol. 20, No. 5, 2004, pp. 947–950. doi:10.2514/1.4997

[7] Li, C., and Kailasanath, K., "Performance Analysis of Pulse Detonation Engines with Partial Fuel Filling," *Journal of Propulsion and Power*, Vol. 19, No. 5, 2003, pp. 908–916. doi:10.2514/2.6183

[8] Radulescu, M. I., and Hanson, R. K., "Effect of Heat Loss on Pulse-Detonation-Engine Flow Fields and Performance," *Journal of Propulsion and Power*, Vol. 21, No. 2, 2005, pp. 274–285. doi:10.2514/1.10286

[9] Owens, Z. C., and Hanson, R. K., "The Influence of Wall Heat Transfer, Friction and Condensation on Detonation Tube Performance," *Combustion, Science & Technology*, Oct. 2009, (to be published).

[10] Cooper, M., and Shepherd, J. E., "Single-Cycle Impulse from Detonation Tubes with Nozzles," *Journal of Propulsion and Power*, Vol. 24, No. 1, 2008, pp. 81–87. doi:10.2514/1.30192

[11] Morris, C. I., "Numerical Modeling of Single-Pulse Gasdynamics and Performance of Pulse Detonation Rocket Engines," *Journal of Propulsion and Power*, Vol. 21, No. 3, 2005, pp. 527–538. doi:10.2514/1.7875

[12] Owens, Z. C., and Hanson, R. K., "Single-Cycle Unsteady Nozzle Phenomena in Pulse Detonation Engines," *Journal of Propulsion and Power*, Vol. 23, No. 2, 2007, pp. 325–337. doi:10.2514/1.22415

[13] Barbour, E. A., and Hanson, R. K., "Analytic Model for Single-Cycle Detonation Tube with Diverging Nozzles," *Journal of Propulsion and Power*, Vol. 25, No. 1, 2009, pp. 162–172. doi:10.2514/1.35420

[14] Fickett, W., and Davis, W. C., *Detonation: Theory and Experiment*, Dover, New York, 2000.

[15] Fickett, W., and Wood, W. W., "Flow Calculations for Pulsating One-Dimensional Detonations," *The Physics of Fluids*, Vol. 9, No. 5, 1966, pp. 903–916. doi:10.1063/1.1761791

[16] Abouseif, G. E., and Toong, T.-Y., "Theory of Unstable Two-Dimensional Detonations: Genesis of the Transverse Waves," *Combustion and Flame*, Vol. 63, No. 1-2, 1986, pp. 191–207. doi:10.1016/0010-2180(86)90120-3

[17] Owens, Z., "Flowfield Characterization and Model Development in Detonation Tubes," Ph.D. Dissertation, Stanford University, Stanford, CA, 2008.

[18] Taylor, G., "The Dynamics of the Combustion Products Behind Plane and Spherical Detonation Fronts in Explosives," *Proceedings of the Royal Society of London A*, Vol. 200, No. 1061, 1950, pp. 235–247. doi:10.1098/rspa.1950.0014

[19] Strang, G., "On the Construction and Comparison of Difference Schemes," *SIAM Journal on Numerical Analysis*, Vol. 5, No. 3, 1968, pp. 506–517. doi:10.1137/0705041

[20] Fedkiw, R. P., Merriman, B., and Osher, S., "High Accuracy Numerical Methods for Thermally Perfect Gas Flows with Chemistry," *Journal of Computational Physics*, Vol. 132, No. 2, 1997, pp. 175–190. doi:10.1006/jcph.1996.5622

[21] Li, H., Owens, Z. C., Davidson, D. F., and Hanson, R. K., "A Simple Reactive Gasdynamic Model for the Computation of Gas Temperature and Species Concentrations behind Reflected Shock Waves," *International Journal of Chemical Kinetics*, Vol. 40, No. 4, 2008, pp. 189–198. doi:10.1002/kin.20305

[22] Liu, X., Osher, S., and Chan, T., "Weighted Essentially Non-Oscillatory Schemes," *Journal of Computational Physics*, Vol. 115, No. 1, 1994, pp. 200–212. doi:10.1006/jcph.1994.1187

[23] Smith, G. P., Golden, D. M., Frenklach, M., Moriarty, N. W., Eiteneer, B., Goldenberg, M., Bowman, C. T., Hanson, R. K., Song, S., Gardiner, W. C. Jr., Lissianski, V. V., and Qin, Z., http://www.me.berkeley.edu/gri_mech/, 1999.

[24] Bates, R. W., Golden, D. M., Hanson, R. K., and Bowman, C. T., "Experimental Study and Modeling of the Reaction $H + O_2 + M \rightarrow HO_2 + M$ ($M = Ar, N_2, H_2O$) at Elevated Pressures and Temperatures between 1050 and 1200 K," *Physical Chemistry Chemical Physics*, Vol. 3, 2001, pp. 2337–2342. doi:10.1039/b010002l

[25] Varatharajan, B., and Williams, F. A., "Ethylene Ignition and Detonation Chemistry, Part 1: Detailed Modeling and Experimental Comparison," *Journal of Propulsion and Power*, Vol. 18, No. 2, 2002, pp. 344–351. doi:10.2514/2.5940

[26] Owens, Z. C., Mattison, D. W., Morris, C. I., and Hanson, R. K., "Flowfield Characterization and Simulation Validation of Multiple-Geometry PDEs Using Cesium-Based Velocimetry," *Proceedings of the Combustion Institute*, Vol. 30, Elsevier, 2005, pp. 2791–2798.

[27] Mattison, D. W., Oehlschlaeger, M. A., Morris, C. I., Owens, Z. C., Barbour, E. A., Jeffries, J. B., and Hanson, R. K., "Evaluation of Pulse Detonation Engine Modeling Using Laser-Based Temperature and OH Concentration Measurements," *Proceedings of the Combustion Institute*, Vol. 30, Elsevier, 2005, pp. 2799–2807.

[28] Tangirala, V. E., Dean, A. J., Chapin, D. M., Pinard, P. F., and Varatharajan, B., "Pulsed Detonation Engine Processes: Experiments and Simulations," *Combustion Science and Technology*, Vol. 176, 2004, pp. 1779–1808. doi:10.1080/00102200490487689

[29] Radulescu, M. I., and Hanson, R. K., "Comment on 'Analytical Model for the Impulse of Single-Cycle Pulse Detonation Tube'," *Journal of Propulsion and Power*, Vol. 20, No. 5, 2004, pp. 956–957. doi:10.2514/1.7876

[30] Wintenberger, E., Cooper, M., Pintgen, F., and Shepherd, J. E., "Reply to Comment on 'Analytical Model for the Impulse of Single-Cycle Pulse Detonation Tube' by M. I. Radulescu and R. K. Hanson," *Journal of Propulsion and Power*, Vol. 20, No. 5, 2004, pp. 957–959. doi:10.2514/1.9441

[31] Owens, Z. C., Mattison, D. W., Morris, C. I., and Hanson, R. K., "Flowfield Characterization and Simulation Validation of Multiple-Geometry PDEs Using Cesium-Based Velocimetry," *Proceedings of the Combustion Institute*, Vol. 30, Elsevier, 2005, pp. 2791–2798.

[32] Du, X., Liu, W. S., and Glass, I. I., "Laminar Boundary Layers Behind Blast and Detonation Waves," UTIAS Report 259, 1982.

[33] Edwards, D. H., Brown, D. R., Hooper, G., and Jones, A. T., "The Influence of Wall Heat Transfer on the Expansion Following a C-J Detonation Wave," *Journal of Physics D: Applied Physics*, Vol. 3, No. 3, 1970, pp. 365–376. doi:10.1088/0022-3727/3/3/317

[34] Boldman, D. R., and Graham, R. W., "Heat Transfer and Boundary Layer in Conical Nozzles," NASA Technical Note, TN D-6594, 1972.

[35] Olson, W. T., "Recombination and Condensation Processes in High Area Ratio Nozzles," *Journal of the American Rocket Society*, Vol. 32, No. 5, 1962, pp. 672–680.

[36] Wintenberger, E., "Application of Steady and Unsteady Detonation Waves to Propulsion," Ph.D. Dissertation, California Institute of Technology, Pasadena, CA, 2004.

[37] Reynolds, W. C., "STANJAN: Interactive Computer Program for Chemical Equilibrium Analysis," Stanford University, No. SUMET-8108, Stanford, CA, Jan. 1986.

[38] Vincenti, W. G., and Kruger, C. H. Jr., *Introduction to Physical Gas Dynamics*, Krieger, Malabar, FL, 1965.

[39] Penner, S. S., "Chemical Reactions during Adiabatic Expansion through a DeLaval Nozzle," *Introduction to the Study of Chemical Reactions in Flow Systems*, Butterworths, London, 1955.

[40] Sangiovanni, J. J., Barber, T. J., and Syed, S. A., "Role of Hydrogen/Air Chemistry in Nozzle Performance for a Hypersonic Propulsion System," *Journal of Propulsion and Power*, Vol. 9, No. 1, 1993, pp. 134–138. doi:10.2514/3.11495

[41] Oosthuizen, P. H., and Carscallen, W. E., *Compressible Fluid Flow*, McGraw-Hill, New York, 1997.

[42] Cooper, M., "Impulse Generation by Detonation Tubes," Ph.D. Dissertation, California Institute of Technology, Pasadena, CA, 2004.

[43] Hill, P. G., and Peterson, C. R., *Mechanics and Thermodynamics of Propulsion*, 2nd ed., Addison-Wesley Longman, Reading, MA, 1992.

J. Powers
Associate Editor